

1. Materials and instrumentation

Warning: The synthesis process may produce toxic gases.

Materials

All the reagents and solvents used for the synthesis were commercially available and used without further purification. All reagents were purchased from **Sinopharm Chemical Reagent Co. Ltd (China)**.

Characterization

The Powder X-ray diffraction (PXRD) acquired using a Rigaku Ultima IV. Scanning electron microscope (SEM, ZEISS MERLIN Compact) and transmission electron microscope (TEM, Talos F200X) were used to observe the morphology. N₂/CO₂ sorption analysis was conducted using Micromeritics ASAP 2020 at 77 K and 273K, using Barrett–Emmett–Teller (BET) calculations for the surface area. X-ray photoelectron spectroscopic (XPS) spectra were collected on a Thermo Scientific Escalab 250 Xi XPS spectrometer. Raman Scattering spectra were recorded with a laser excitation wavelength of 532 nm. The CO₂-TPD test was investigated by Micromeritics AutoChem II 2920 chemisorption instrument. The electro-catalysis reactions were tested by a Model CHI 760E workstation (CH Instruments, Chenhua, Shanghai, China) and RRDE-3A (ALS Co., Ltd). X-ray absorption spectroscopy (XAS) experiments were performed at the Beijing Synchrotron Radiation Facility (BSRF, soft Xray beamline) and the National Synchrotron Radiation Laboratory (NSRL, XMCD beamline). Hydrocarbons were tested by a flame ionization detector (FID). A thermal conductivity detector (TCD) was used to detect hydrogen, oxygen and CO with nitrogen as the carrier gas. Liquid products were collected from the cathode chambers after electrolysis and quantified by NMR (Bruker AVANCEAV III 400) spectroscopy.

Fabrication of ZnO NPs solution. 0.38g Zn(CH₃COO)₂·2H₂O were added to 35 mL ethanol solution and magnetic stirred until the solution turned to clarifying. Then, 1.5 mL KOH (0.17g)-ethanol solution was added into the above solution under magnetic stirred at 80°C for 12 min.

Fabrication of ZIF-8. 0.74g Zn(NO₃)₂·6H₂O and 1.63g 2-methylimidazole (2-MeIM) were dissolved in 50 mL of ethanol and magnetic stirred for 24 h at room temperature. The product was collected by centrifuge (6000 rpm, 5 min) and washed three times by ethanol. Finally, the product was dried in vacuum at 60°C for 6 h.

Fabrication of PC. PC catalyst was prepared via carbonization of 1 g ZIF-8 powders at 900 °C for 2 h under N₂ gas flow with heating rate of 5°C min⁻¹. The products in turn were washed by 10% HF aqueous solution, 10% HCl aqueous solution, deionized water, absolute ethanol and acetone, respectively.

Fabrication of ZnO NP@ZIF-8. 0.14g Zn(NO₃)₂·6H₂O was added to 10 mL ethanol, meanwhile 0.16g 2-methylimidazole (2-MeIM) was dissolved in 5 mL of ethanol. At first, 10 mL Zn(NO₃)₂·6H₂O ethanol solution was added into above ZnO NPs solution (35mL), then 5 mL of 2-MeIM ethanol solution was poured into above solution.

Finally, the mixture solution was magnetic stirred for 24 h and collected by centrifuge (6000 rpm, 2 min). The final products were dried in vacuum at 60°C for 6 h.

Fabrication of ZnO NP@ZIF8-W. 0.14g Zn(NO₃)₂·6H₂O was dissolved in 10 mL ethanol, meanwhile 0.16g 2-methylimidazole (2-MeIM) was dissolved in 5 mL of ethanol. Then 10 mL of Zn(NO₃)₂·6H₂O ethanol solution was added into above ZnO NPs solution firstly with magnetic stirred at the room temperature, and then 5 mL of 2-MeIM ethanol solution was poured into the above solution as well. Finally, the mixture solution was magnetic stirred for 24 h. The product was collected by centrifuge (6000 rpm, 2 min), the product was washed by EtOH: Deionized Water=1:1 solution 2 hours to remove KNO₃ and then dried in vacuum at 60°C for 6 h.

Fabrication of DHPC and HPC electro-catalyst. DHPC catalyst was prepared via direct carbonization of 1 g ZnO@ZIF-8 or ZnO@ZIF8-W powders at 900°C for 2h under N₂ gas flow with heating rate of 5 °C min⁻¹ (keep 300 °C for 30min). And the catalyst for XPS, electrochemical catalyst, N₂ sorption and Raman spectrum testing were washed by 10% HF aqueous solution, 10% HCl aqueous solution, deionized water, absolute ethanol and acetone for 6 h, respectively. Finally, the products were dried in vacuum at 60°C for 12 h. 2g ZnO NP@ZIF-8 or ZnO NP@ZIF8-W are pyrolyze at 500°C/600°C for 2h, named DHPC (500), DHPC (600), HPC (500) and HPC (600). (Note: Using 10% HF aqueous solution is aim to eliminate SiO₂ impurity which comes from quartz tube)

H⁺ Adsorption Measurements.

The proton (H⁺) adsorptivity of DHPC and HPC was studied by dialysis. 50mg of DHPC (or HPC) was added to a 10 mL 5 mM HCl solution. The DHPC (or HPC) solution was dialyzed using a semipermeable membrane in a 5mM HCl (500 mL) dialysate. The dialysate was stirred and then 2mL dialysate was taken out for analysis at pre-designed time interval. The obtained HCl dialysate was titrated using a 5mM NaOH solution, thus the relationship between the concentration of the dialysate HCl solution and the time can be reached.

The adsorption quantity of H⁺ (Q_H^+ , mg) was calculated using the following formula:

$$Q_H^+ = \frac{(C_0 - C_e) \times V}{1000/36.46}$$

Where C₀ and C_e are the original and temporal HCl concentrations (mg L⁻¹) respectively, V is the volume of HCl solution (500-2n mL, n is the number of temporal measurements), and 36.46 is the molecular weight of HCl.

Electrochemical measurements of CO₂RR

Linear sweep voltammetry experiments were performed using a standard three-electrode configuration. A platinum wire was used as an encounter electrode and a saturated calomel electrode (SCE) was used as a reference electrode. The working electrode was either a catalyst modified glassy carbon disk electrode (GCE, 3.0 mm diameter CH Instruments) (LSV test), or a catalyst modified carbon fiber paper electrode (0.7 cm × 0.7 cm) (faradic efficiency test). 3 mg was added into 0.5 mL 0.5 % Nafion solution. After sonication, 0.4 mL dispersed solution was dropped directly onto a 0.7 cm × 0.7 cm carbon paper (double sides). 2.5 mg electro-catalyst was added into 1 mL 0.5 % Nafion solution. After sonication, 4 μL dispersed solution was dropped on glassy carbon disk electrode (diameter, 3 mm).

The mass density of catalyst was 0.14 mg cm⁻². For product analysis, the bulk electrolysis was performed in an airtight electrochemical H-type cell with a catalyst modified carbon fiber paper electrode (0.7 cm × 0.7 cm) as the work electrode. In addition, an electrochemical test was used with the catalyst modified glassy carbon disk electrode as the work electrode. Initially, polarization curves for the modified electrode were carried out under an inert Ar (gas) atmosphere. After this, the solution was purged with CO₂ (99.999%) for 30 min (CO₂-saturated 0.5 M KHCO₃ high purity aqueous (PH=7.2)/ CO₂-saturated real sea water (PH=5.3) and the electro-catalytic CO₂ reduction was measured. The constant-potential electrolysis experiments were performed in an airtight electrochemical H-type cell with three electrodes and two compartments (volume of each part is 115 mL) separated by a Nafion®212 anion exchange membrane with 75 mL 0.5 M KHCO₃ electrolyte in each chamber.

CO₂ Reduction Reaction products Analysis

The bulk electrolysis was further performed in an airtight electrochemical H-type cell with 75 mL 0.5 M KHCO₃/Original sea water electrolyte in each chamber. For detection of gas products, hydrocarbons (CH₄, C₂H₄, and C₂H₆) were tested by a flame ionization detector (FID) with helium as the carrier gas. A thermal conductivity detector (TCD) was used to detect hydrogen, oxygen (collected from anode) and CO with nitrogen as the carrier gas. Cathodic gas sample was injected into two aliquots for GC analysis equipped with a TCD detector. One aliquot was routed through a packed MoleSieve 5A column and another was routed through a packed HP-PLOT Q column before passing a thermal conductivity detector (TCD) for CO quantification. The liquid products were collected from the cathode chambers after electrolysis and quantified by NMR (Bruker AVANCEAV III 400) spectroscopy, in which 0.5 mL electrolyte was mixed with 0.1 mL D₂O (deuterated water) and 0.1 μL dimethyl sulfoxide (DMSO, Sigma, 99.99%) was added as an internal standard.

The calculation of Faradaic efficiency by the equation 1 and 2:

For CO,

$$FE = \frac{2F \times n_{CO}}{I \times t} \times 100\% \quad (1)$$

For H₂,

$$FE = \frac{2F \times n_{H_2}}{I \times t} \times 100\% \quad (2)$$

where F is the Faraday constant, η(CO) is the moles of produced CO, and η(H₂) is the moles of produced H₂.

The fabrication of XAS samples (CO₂RR)

Pristine Sample: DHPC sample without any extra treatment.

CO₂-saturated: At first, 10mg C-900 was dispersed in 4 mL of ethanol-distilled water (1:1) aqueous solution by sonication. Then above 4 mL catalyst ink was dropped onto the carbon fiber paper (0.7 cm × 0.7 cm, double side) and dried under ambient condition. Then, the above carbon fiber paper was immersed into CO₂-saturated 0.3M KHCO₃

solution and washed by deionized water carefully. Finally, the electro-catalyst sample was collected by centrifuge (8000 rpm, 1 min) and dried at 25 °C for 24h.

CO₂RR Middle (LSV): The carbon fiber paper electrode served as working electrode. Linear sweep voltammetry experiments were performed using a standard three-electrode configuration. Notably, the LSV test was stopped at the half-wave potential (-0.6V vs. RHE) and then the working electrode was taken out. The working electrode was washed by deionized water carefully. Finally, the electro-catalyst sample was collected by centrifuge (8000 rpm, 1 min) and dried at 25 °C for 24h.

CO₂RR Finished (LSV): Linear sweep voltammetry experiments were performed using a standard three-electrode configuration. The LSV test was stopped at the finished potential (-1.2 V vs. RHE) and then the working electrode was taken out. The working electrode was washed by deionized water carefully. Finally, the electro-catalyst sample was collected by centrifuge (8000 rpm, 1 min) and dried at 25 °C for 24h.

Calculation method

The computations were implemented by the Vienna ab initio simulation package (VASP) based on density functional theory (DFT) to optimize the structure and investigate the reaction mechanisms. Projector augmented waves (PAW) was used to depict the ion-electron interactions when the function of Perdew, Burke and Ernzerhof (PBE)^[1] based on the generalized gradient approximation (GGA) was adopted to describe the exchange and correlation potential. In structure optimization calculations, 3×1×1 Monkhorst-Pack^[2] sampled k points were used, and a cut-off energy of 400 eV was adopted. For density of states (DOS) plotting, a larger set of k points (11×11×11) was used. The threshold of convergence was set to 1×10⁻⁴ eV and 0.01 eV/Å for the self-consistent field (SCF) and ion steps, respectively. In all the investigated slab models, the vacuum space is set to be at least 17 Å to separate the interaction between neighboring slabs. Spin polarization was considered in all the computations. The corresponding free energy was calculated as $\Delta G = \Delta E + \Delta ZPE - T\Delta S$, where ΔE , ΔZPE , T and ΔS is the DFT derived energy, zero point energy, the temperature in Kelvin and entropy, respectively. The solvent effect for *COOH and *CO was -0.25 and -0.10 eV, with a correction of 0.51 eV for gas-phase CO. ^[3]

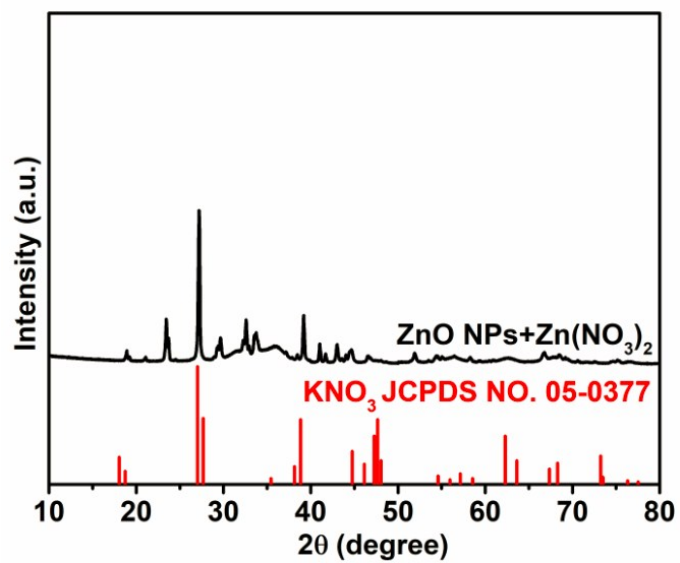


Figure S1. The XRD patterns of ZnO-EtOH solution adding Zn(NO₃)₂. As shown in synthesis process, a lot of K ions exist in the ZnO-EtOH solution. Thus, introducing NO₃⁻ anions can prompt the formation of KNO₃.

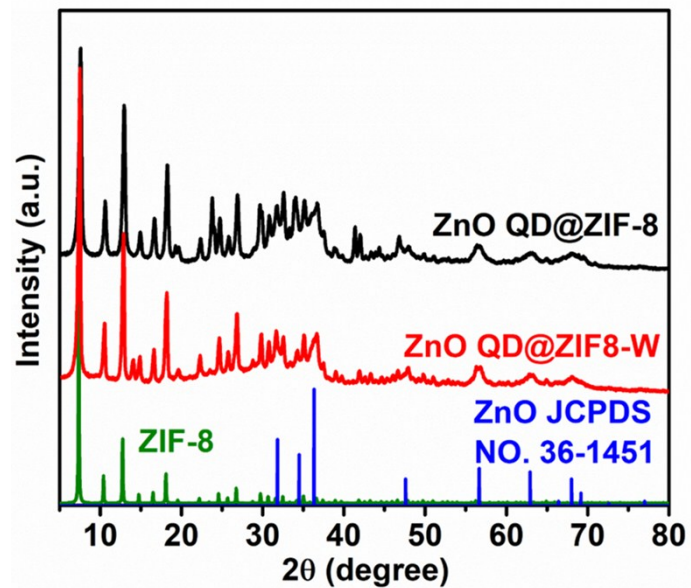


Figure S2. (a), The PXRD patterns of ZnO NP@ ZIF-8 and ZnO NP@ZIF8-W.

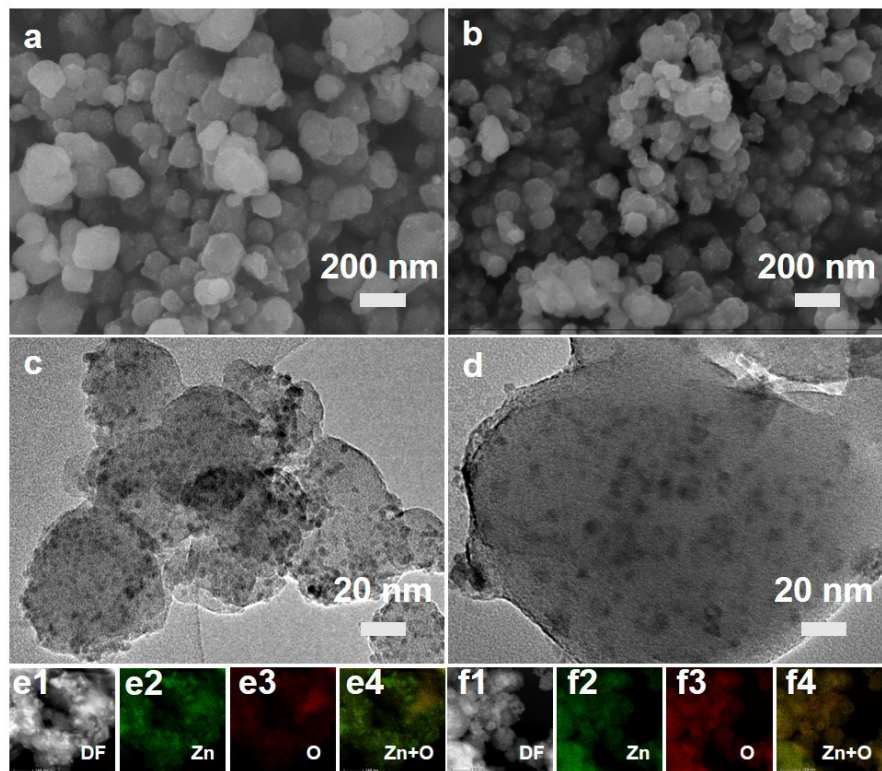


Figure S3. (a), SEM image of ZnO NP@ZIF-8. (b), SEM image of ZnO NP@ZIF8-W. (c), TEM image of ZnO@ZIF-8. (d), TEM image of ZnO NP@ZIF8-W. (e1-e4), The element mappings of ZnO@ZIF-8. (f1-f4), The element mappings of ZnO NP@ZIF8-W. Scanning electron microscopy (SEM) images show that ZnO NP@ZIF-8 and ZnO@ZIF8-W sample are the composite of ZnO NPs and ZIF-8 nanocrystals with similar morphology features (Figure. S3a, S3b). Transmission electron microscope (TEM) suggests ZnO NPs have uniform particle size (3-5nm) and be embedded in ZIF-8 nanocrystals homogeneously (Figure S3c, 3d). The element mappings (Figure S3e, 3f) of ZnO NP@ZIF-8 and ZnO NP@ZIF8-W exhibit homogeneous oxygen elemental distribution over the entire architecture, which also demonstrate the well dispersion of ZnO NPs.

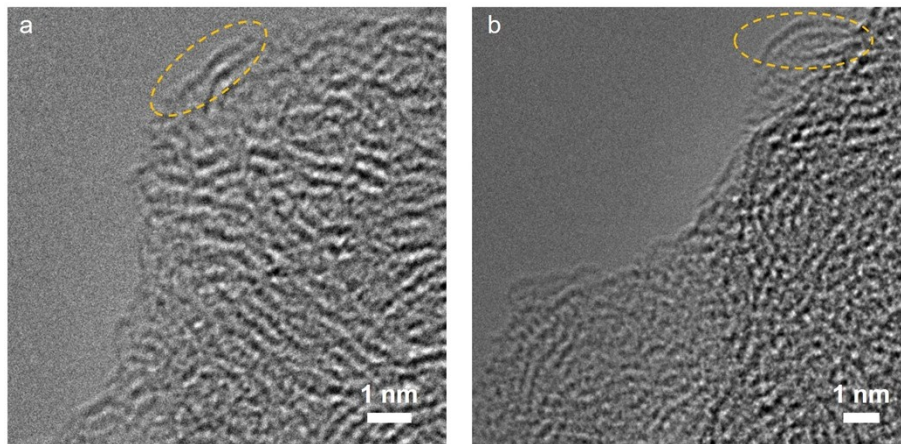


Figure S4. (a, b) High Resolution Transmission Electron Microscopy (HRTEM) of HPC. The HRTEM images of HPC show thin but blurry edge (yellow area), so the atomic array of carbon can't be identified. But, have many zigzag/armchair structures in edge can be seen.

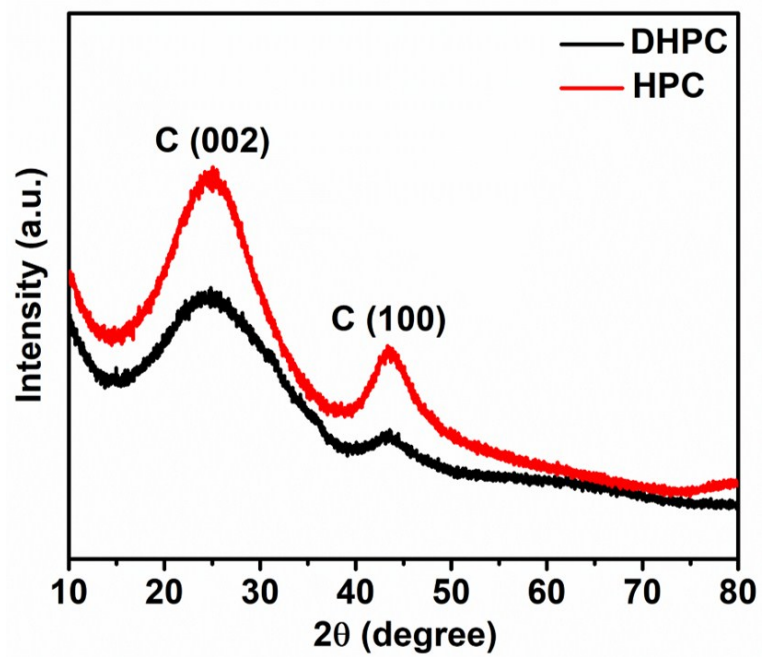


Figure S5. Power X-ray Diffraction pattern of DHPC and HPC.

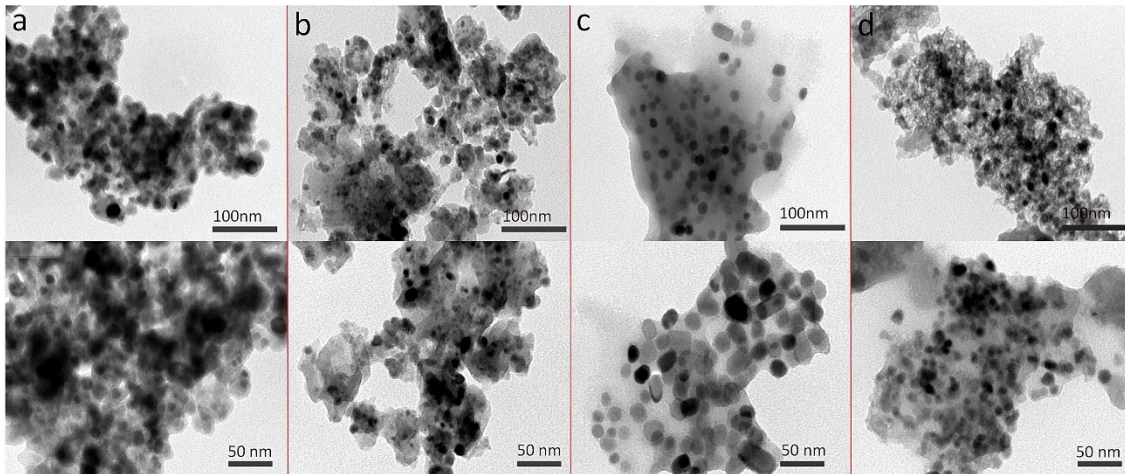


Figure S6. (a) TEM images of DHPC (500); (b) TEM images of HPC (500); (c) TEM images of DHPC (600); and (d) TEM images of HPC (600).

As shown in above figures, both DHPC (500) and DHPC (500) show larger ZnO particles than that of DHPC (600) and HPC (600), indicating KNO_3 can intensify the oxidation of Zn ions and aggregation of ZnO, resulting larger ZnO template. The possible reactions are proposed in the following:



In higher pyrolytic temperature, ZnO consumes plenty of carbon by carbon thermal reduction process, constructing larger mesopores and inhibiting ordering graphitization, which are beneficial to the defect sites fabrication. The possible reactions are proposed in the following:



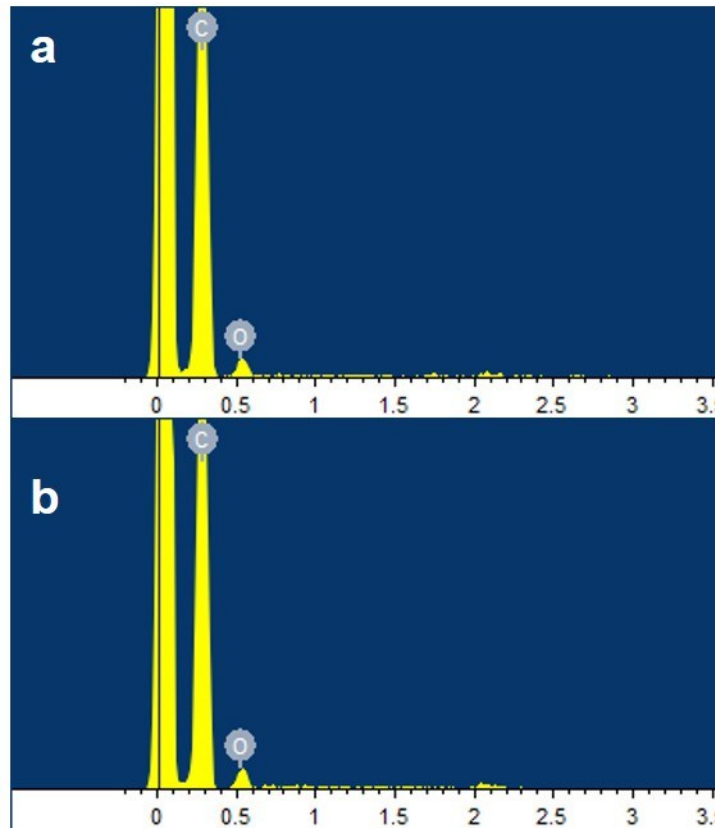


Figure S7. (a), The EDS spectrum of DHPC. (b), The EDS spectrum of HPC.

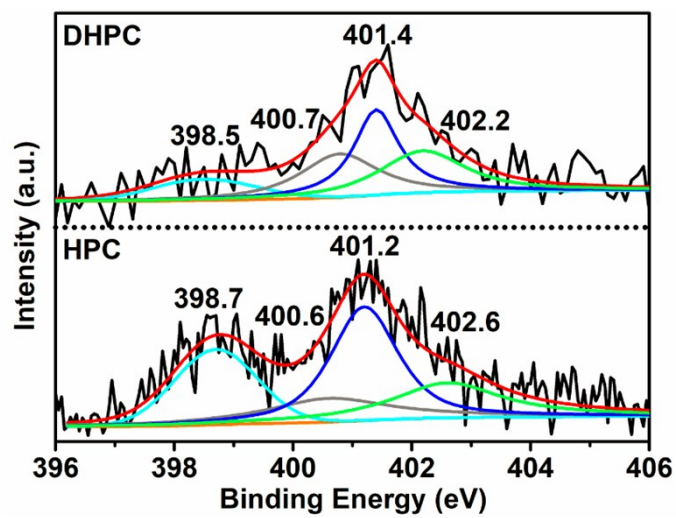


Figure S8. N 1s XPS spectra of DHPC and HPC.

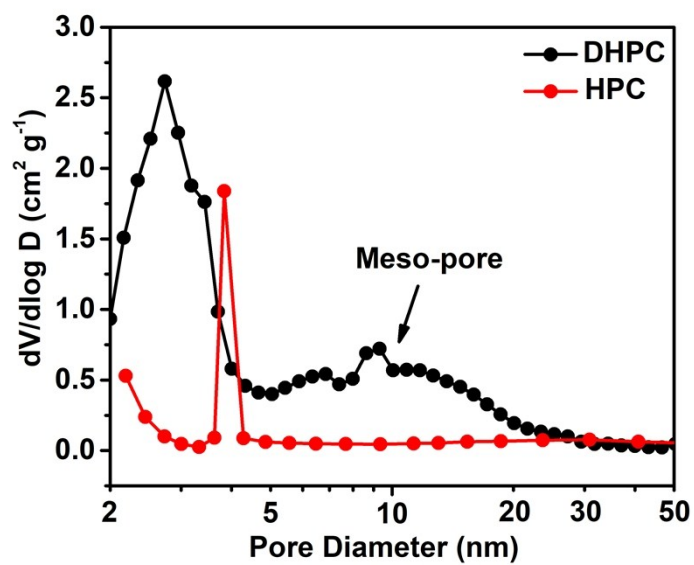


Figure S9. The pore distributions of DHPC and HPC at meso-pore area (>2nm), and the pore size distributions are based on adsorption branch.

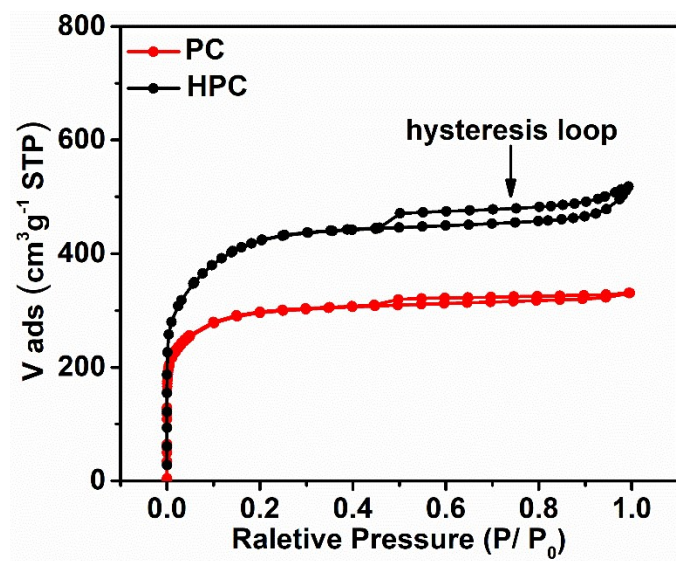


Figure S10. N_2 adsorption isotherms of porous carbon materials of HPC and PC at 77 K.

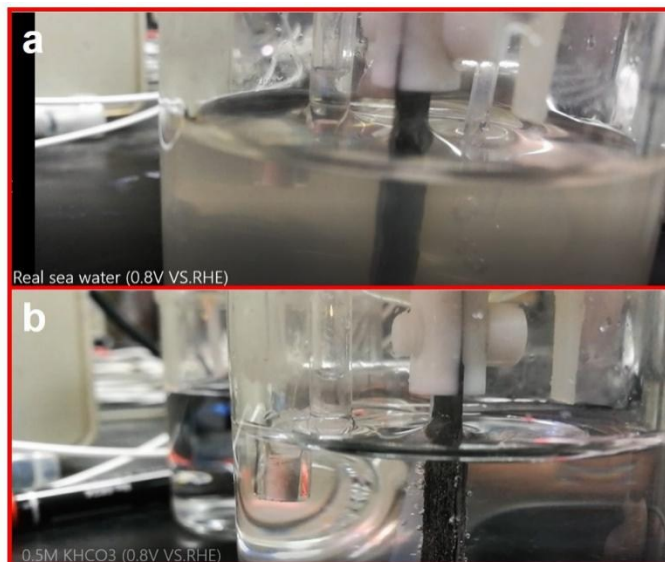


Figure S11. (a), The photo of CO₂RR test under real sea water medium. (b), The photo of CO₂RR test under 0.5 M KHCO₃ medium.

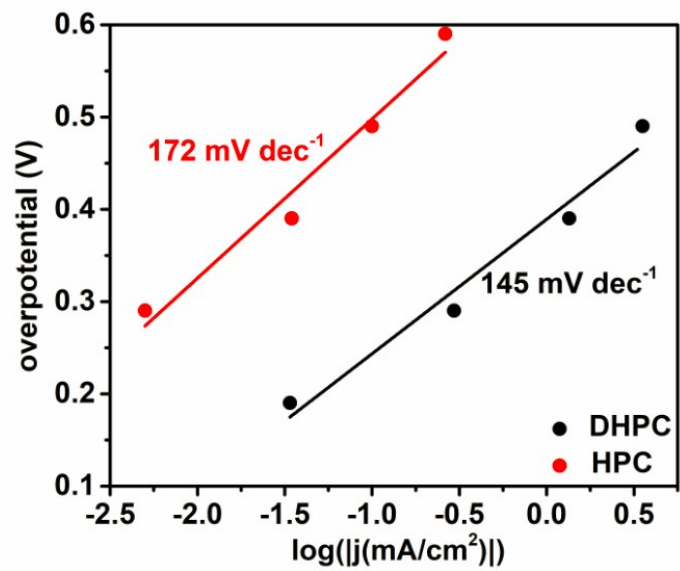


Figure S12. The Tafel slopes of DHPC and HPC in the CO_2 -saturated 0.5 M KHCO_3 solution

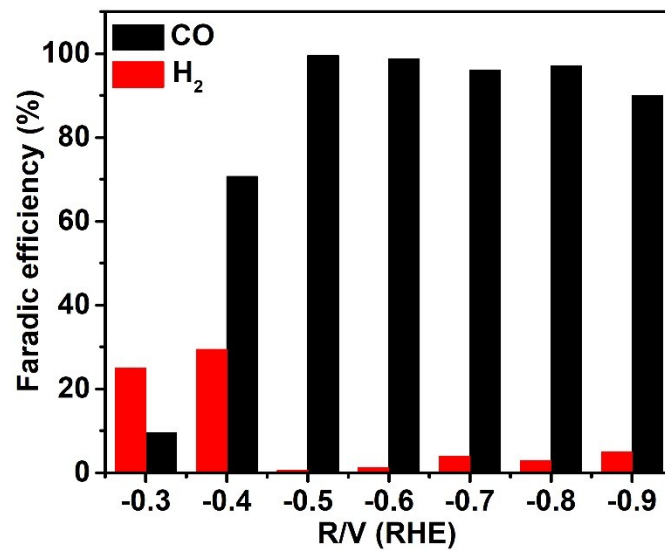


Figure S13. (a), CO-FEs (black) and H₂-FEs (red) of DHPC in the CO₂-saturated 0.5M KHCO₃ solution. Notably, the CO faradic efficiency achieves 10% just in -0.3 V, which means an ultra-low overpotential of DHPC.

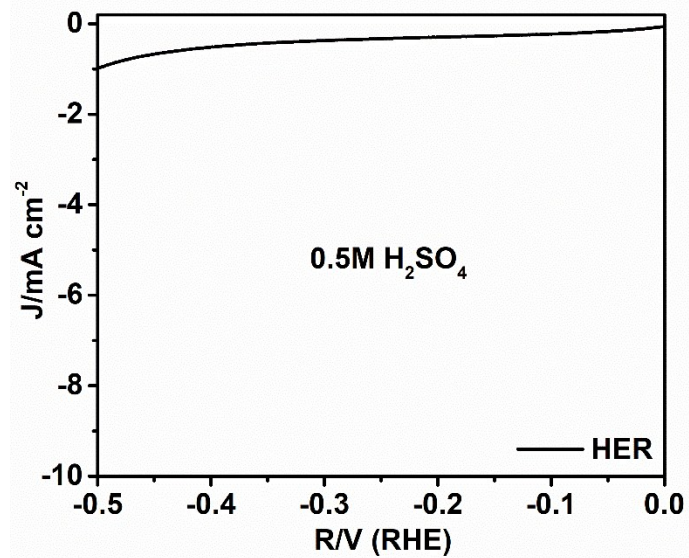


Figure S14. The HER performance of DHPC in 0.5 M H₂SO₄ medium.

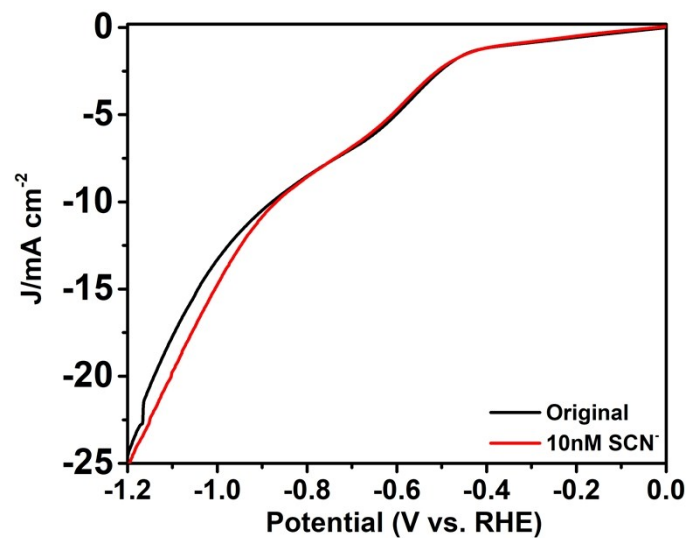


Figure. S15 LSV curves of DHPC in 0.5 M KHCO₃ and 0.5 M KHCO₃+10 mM KSCN electrolyte.

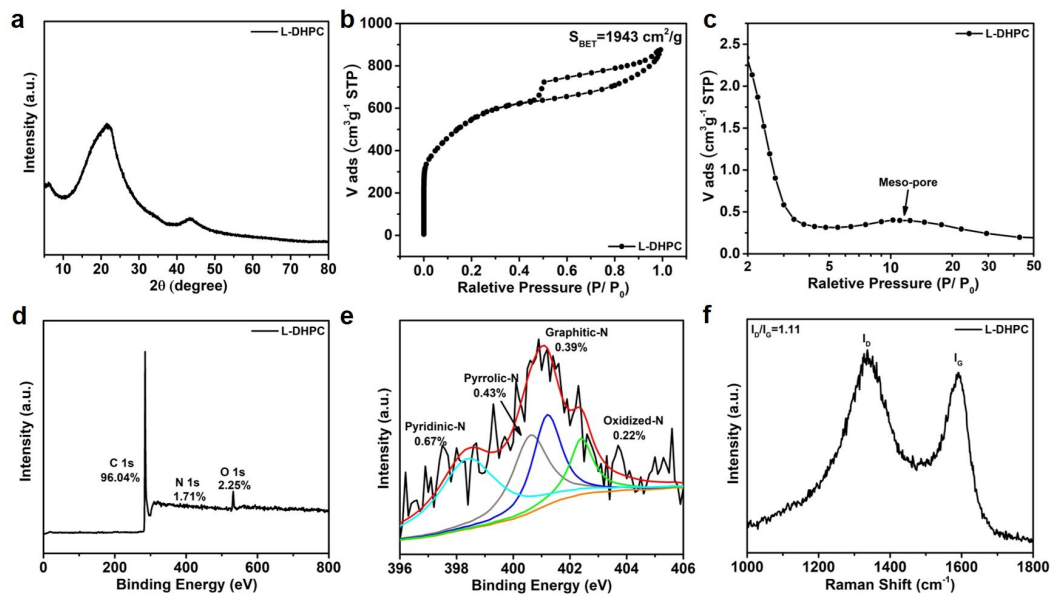


Figure S16. (a), Power X-ray Diffraction pattern of L-DHPC. (b), N_2 sorption isotherms of hierarchical porous carbon materials of L-DHPC at 77 K. (c), The pore distribution of L-DHPC at meso-pore area ($>2\text{nm}$), and the pore size distribution is based on adsorption branch. (d), XPS survey scan of L-DHPC. (e), N 1s XPS spectrum of L-DHPC. (F), Raman spectrums of L-DHPC.

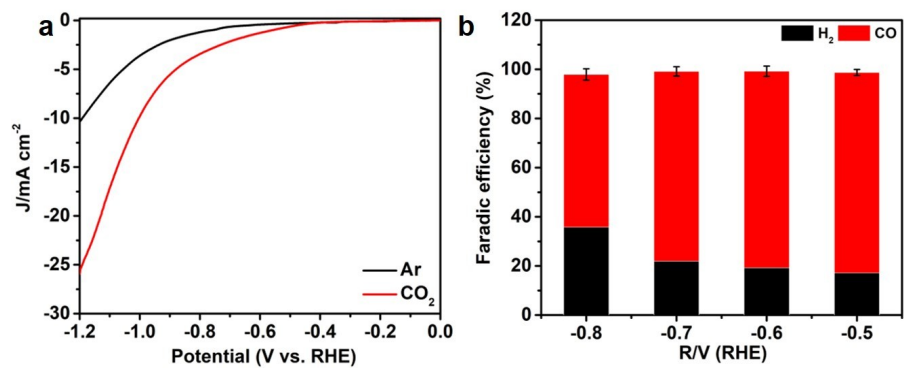


Figure S17. (a), LSV curves of L-DHPC in 0.5 M KHCO₃ electrolyte. (b), Faradaic efficiencies of L-DHPC in 0.5 M KHCO₃ at various potentials.

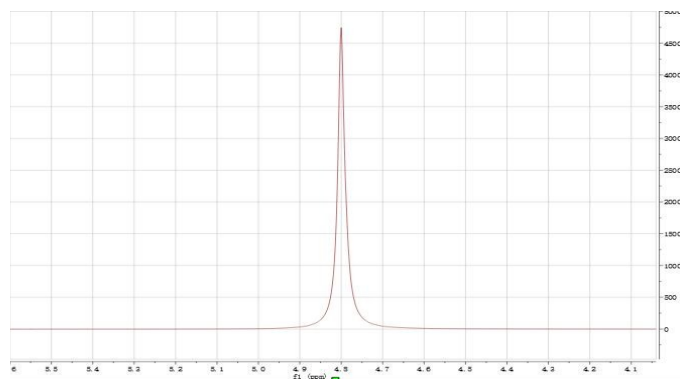


Figure S18. ^1H NMR image of CO_2RR electrolyte, in which DHPC serve as electro-catalyst. As shown in above image, ^1H NMR data just exhibits a characteristic peak of D_2O at 4.8 ppm and without any other reduction liquid products.

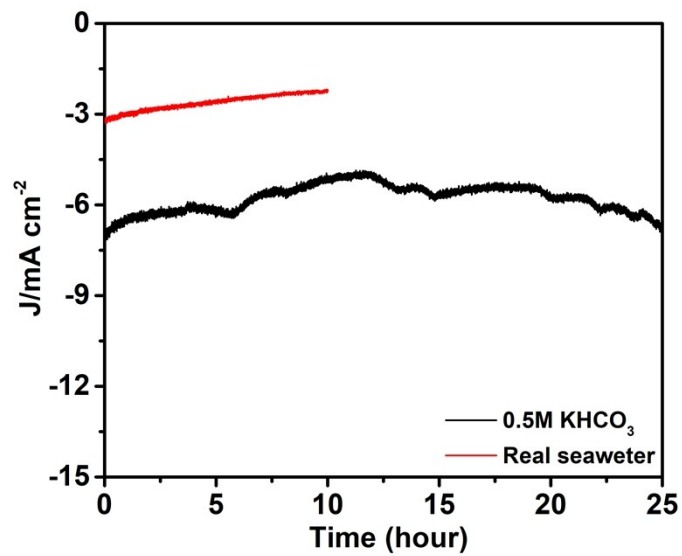


Figure S19. The i-t curves of DHPC (applied potential: -0.8V vs. RHE) in CO₂-saturated 0.5 M KHCO₃ and real sea water medium.

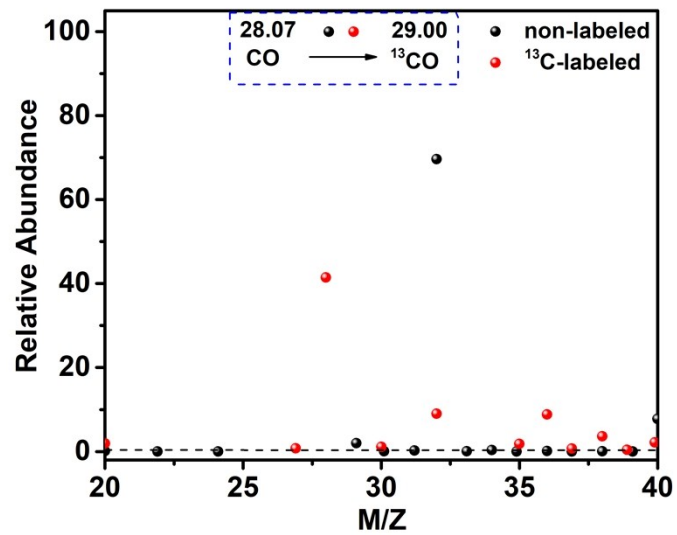


Figure S20. GC-MS spectra of the CO products over DHPC at -0.8 V (vs. RHE) with nonisotope-labeled CO_2 and $^{13}\text{CO}_2$ as the feedstock, respectively.

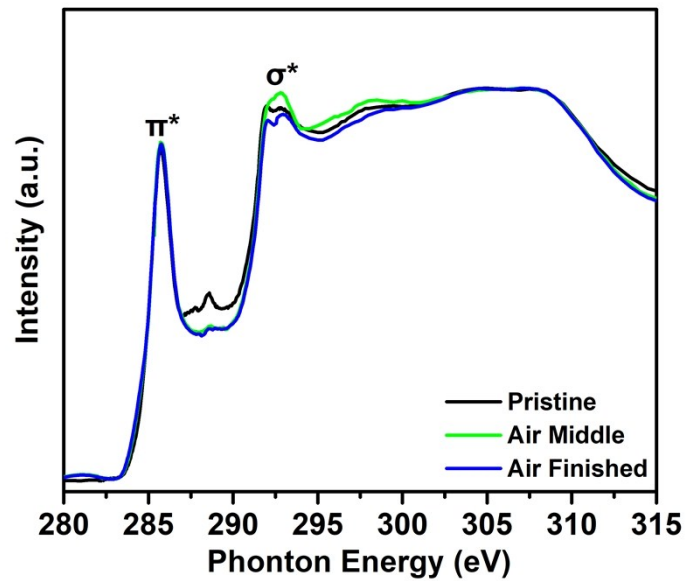


Figure S21. K-edge XAS curves of DHPC with different treatment modes in air condition.

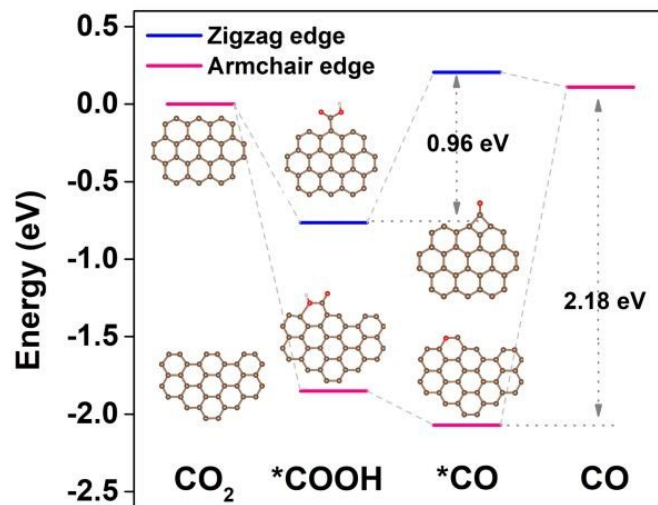


Figure S22. The DFT calculated free energy diagram of zigzag and armchair edge model.

3. Supplementary Tables

Table S1. Comparison of the C, N, O ratios in DHPC and HPC from left to right (based on XPS).

	C (Atomic %)	N (Atomic %)	O (Atomic %)
DHPC	96.95%	0.95%	2.10%
HPC	96.36%	2.21%	1.34%

Table S2 Inductively Coupled Plasma (ICP) test of DHPC and HPC.

Element	DHPC (ppm)	HPC (ppm)
Zn	0.1649	0.2103
K	0.1383	0.1522
Fe	0.2098	0.2517
Co	0.0039	0.0023
Pt	0.0062	0.0074

Table S3. Element distribution (based on EDS) of DHPC and HPC.

	C (Atomic %)	N (Atomic %)	O (Atomic %)
DHPC	93.56	N/A	6.44
HPC	93.73	N/A	6.27

Table S4. Comparison of type and ratios of N in DHPC and HPC from left to right (based on XPS).

	DHPC (Atomic %)	HPC (Atomic %)
Pyridinic-N	0.12%	0.51%
Pyrrolic-N	0.25%	0.36%
Graphite-N	0.30%	0.84%
Oxidized-N	0.27%	0.48%

Table S5. The adsorption energies of CO₂ and H⁺ in C5+H.

C5+H	H ⁺	CO ₂
Free Energy (eV)	-0.78	-0.46

Table S6. The Gibbs free energies of CO₂* and H* in C5+H.

C5+H	H*	CO ₂ *
Free Energy (eV)	-0.361	0.258

The free energies for H* and CO₂* of C5+H are -0.361 and 0.258 eV, respectively. These results show that the rate-determining step of C5+H model in CO₂RR process is COOH* hydrogenation step with 0.33 eV Gibbs free energy, which is lower than that of HER (0.36 eV). Therefore, these results indicate a more favorable CO₂RR than HER.

Table S7. Comparison of the CO₂RR performance (CO product) in the literatures.

Catalyst	Electrolyte Real Sea Water	Electrolyte Na/KHCO ₃	Potential RHE [V]	vs.	Main Production [FE%]	Ref.
DHPC	N/A	0.5 M KHCO ₃	-0.5V		CO (99.5%)	This Work
DHPC	Real seawater	-	-0.5V		CO (96.5%)	This Work
Au₂₅ cluster	N/A	0.1M KHCO ₃	-0.89 V		CO (99.6%)	<i>J. Am. Chem. Soc.</i> , 2012, 134 , 10237.
Au NPs 8 nm	N/A	0.5M KHCO ₃	-0.67 V		CO (90%)	<i>J. Am. Chem. Soc.</i> , 2013, 135 , 16833.
Nanoporous Ag	N/A	0.5M KHCO ₃	-0.6 V		CO (92%)	<i>Nat. Comm.</i> , 2014, 5, 3242.
Cu NPs 13.1 nm	N/A	0.1M KHCO ₃	-1.1 V		H ₂ 0.078, CO 0.016, CH ₄ 0.0018, C ₂ H ₄ 0.0006 (Vol. % cm ⁻²)	<i>J. Am. Chem. Soc.</i> , 2014, 136 , 6978.
Au NWs	N/A	0.5M KHCO ₃	-0.35 V		CO (94%)	<i>J. Am. Chem. Soc.</i> , 2014, 136, 16132.
Nitrogen -doped CNTs	N/A	0.1 M KHCO ₃	-0.26 V		CO (80%)	<i>ACS Nano</i> , 2015, 9 , 5364.
Au/carbon nanotubes (CNT)	N/A	0.5M NaHCO ₃	-0.5 V		CO (94%)	<i>J. Am. Chem. Soc.</i> , 2015, 137, 4606.
Anodized polycrystalline Ag	N/A	0.1M KHCO ₃	-0.8 V		CO (89%)	<i>ACS Nano</i> , 2015, 9 , 5364.
g-C₃N₄/CNT	N/A	0.1M KHCO ₃	-0.75V		CO (60%)	<i>Chem. Eur. J.</i> , 2016, 22 , 11991-11996.
N-3D graphene	N/A	0.1M KHCO ₃	-0.58V (vs. SHE)		CO (85%)	<i>Nano Lett.</i> , 2016, 16 , 466
3D porous hollow fiber Cu	N/A	0.3M KHCO ₃	-0.4 V		CO 75%	<i>Nat. Comm.</i> , 2016, 7, 10748.
Oxide-derived Ag	N/A	0.1M KHCO ₃	-0.8 V		CO (89%)	<i>Angew. Chem. Int. Ed.</i> , 2016, 55 , 9748
Meso- structured Ag	N/A	0.1M KHCO ₃	-0.7 V		CO (>80%)	<i>Angew. Chem. Int. Ed.</i> , 2016, 55 , 15282.
Pd Icosahedra/C	N/A	0.1M KHCO ₃	-0.8 V		CO (91.1%)	<i>Angew. Chem. Int. Ed.</i> , 2017, 56 , 3594.

Ni-N₄-C	N/A	0.5M KHCO ₃	-0.81 V	CO (99%)	<i>J. Am. Chem. Soc.</i> , 2017, 139 , 14889.
CN-H-CNT	N/A	0.1M KHCO ₃	-0.5 V	CO (≈88%)	<i>Adv. Energy Mater.</i> , 2017, 7 , 1701456.
Cu/SnO₂ NPs	N/A	0.5M KHCO ₃	-0.7 V	CO (93%)	<i>J. Am. Chem. Soc.</i> , 2017, 139 , 4290.
LiET-Zn	N/A	0.1M KHCO ₃	-1.17 V	CO (91.1%)	<i>ACS Nano</i> , 2017, 11 , 6451.
Fe-N-C	N/A	0.1M KHCO ₃	-0.6 V	CO (85%)	<i>Chem. Sci.</i> , 2018, 9 , 5064.
Ni-SAC	N/A	1 M KHCO ₃	-1.03 V	CO (98%)	<i>Energy Environ. Sci.</i> , 2018, 11 , 1204.

Table S8. Comparison of the CO₂RR maximal partial current density (CO product) in the literatures.

Catalyst	Electrolyte Na/KHCO₃	Potential RHE [V]	vs.	maximal CO₂RR partial current density (mA cm⁻²)	Ref.
DHPC	0.5 M KHCO ₃	-0.8V		6.2	This Work
DHPC	-	-0.8V		0.4	This Work
Ni-N₄-C	0.5M KHCO ₃	-1.0V		7.3	<i>J. Am. Chem. Soc.</i> , 2017, 139 , 14889.
Fe-N-C	0.1M KHCO ₃	-0.8V		5	<i>Chem. Sci.</i> , 2018, 9 , 5064.
O-AuCu	0.5 M KHCO ₃	-0.77		1.39	<i>J. Am. Chem. Soc.</i> 2017, 139 , 248329-8336

References

- (1) J. P. Perdew, K. Burke, and M. Ernzerhof. *Phys. Rev. Lett.* 77 (1996) 3865.
- (2) H. J. Monkhorst, and J. D. Pack, *Phys. Rev. B* 13 (1976) 5188.
- (3) A. A. Peterson, F. A. Pedersen, F. Studt, J. Rossmeisla and J. K. Nørskov, *Energy & Environmental Science* 3 (2010) 1311.